Available online at www.derpharmachemica.com

Scholars Research Library

Der Pharma Chemica, 2015, 7(12):103-121
(http://derpharmachemica.com/archive.html)

ISSN 0975-413X
CODEN (USA): PCHHAX

A quantum-chemical analysis of the antiproliferative activity of *N*-3-benzimidazolephenylbisamide derivatives against MGC803, HT29, MKN45 and SW620 cancer cell lines

Juan S. Gómez-Jeria* and Javier Valdebenito-Gamboa

Quantum Pharmacology Unit, Department of Chemistry, Faculty of Sciences, University of Chile. Las Palmeras 3425, Santiago, Chile

---

ABSTRACT

A Density Functional Theory analysis was performed to find relationships between the electronic structure of a group of N-3-benzimidazolephenylbisamide derivatives and their antiproliferative activity against MGC803, HT29, MKN45 and SW620 cancer cell lines. The geometries were fully optimized at the B3LYP/6-31G(d,p) level. A similar skeleton for all the molecules, composed by 38 atoms, was used for the analysis. Statistically significant equations were obtained for the four cell lines. The equivalent 2D pharmacophores were built and some ring-ring interactions were suggested. The question of knowing if the role of the C-E rings connector is the same for all the cases analyzed here cannot be fully answered yet. The analysis of the equations and the pharmacophores should offer information about new probable substitution sites.

INTRODUCTION

In the field of cancer drug design, a crucial early-stage element frequently involves the screening of compounds in cell-based *in vitro* assays. One of the most common parameters measured is the impact of a given molecule on the proliferation of a cancer cell line. Many experimental work was carried out with different molecular systems ands cell lines [1-30]. Theoretical work was also performed [31]. In previous papers we have carried out studies relating electronic structure with antiproliferative activity and cytotoxicity for different series of molecules [32-36]. We present here the results of a Density Functional Theory study of the relationships between the electronic/molecular structure and the antiproliferative activity on MGC803, HT29, MKN45 and SW620 cancer cell lines by a family of recently synthesized *N*-3-benzimidazolephenylbisamide derivatives [5] We expect that these results will provide new information for an improved understanding of the action mechanism and for the synthesis of new derivatives.

MATERIALS AND METHODS

The QSAR method

Since the method employed here has been described in a very exhaustive mode in practically each paper we have published on this topic, we decided to refer the reader to the literature [37-44]. Consequently, we shall discuss below only the resultant equations. The master equation linking any biological activity with the electronic structure is the only member of the class of model-based methods [45]. It encompasses local atomic reactivity indices describing virtually all possible atom-atom interactions. In the case of *in vitro* ligand-site interactions expressed as equilibrium constants or IC_{50} values this method produced outstanding results. In the case of an *in vivo* or *in vitro* multistep and/or multimechanistic action mechanism our technique necessitates that all the steps and all the mechanisms inside every step be the same for all the group of molecules under analysis [36]. Very good results were obtained for a diversity of molecules and biological activities ([32-35, 44, 46-69] and references therein). This approach is called

the Klopman-Peradejordi-Gómez method (KPG). Regarding the resulting statistical equations, we must remember that the variation of the numerical values of the local atomic reactivity indices (LARIs) appearing inside them explains the variation of the antiproliferative activity throughout the series. Therefore, any LARI making a constant contribution will not appear explicitly inside these equations.

Selection of molecules and biological activity.

The molecules were selected from a recent study and are shown in Table 1 and Fig. 1.

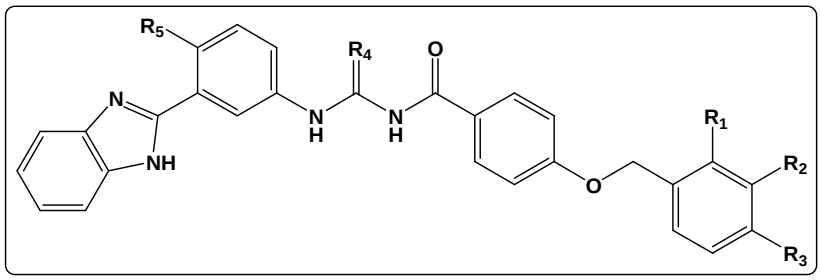

Figure 1. General formula of the selected *N*-3-benzimidazolephenylbisamide derivatives

Table 1. Selected *N*-3-benzimidazolephenylbisamide derivatives

Mol.	R_1	R_2	R_3	R_4	R_5
1	H	H	H	S	Me
2	H	Cl	H	S	Me
3	H	H	CF_3	S	Me
4	H	CF_3	H	S	Me
5	F	H	H	S	Me
6	Cl	Cl	H	S	Me
7	H	H	Me	S	Me
8	H	F	H	S	Me
9	Cl	H	H	S	Me
19	H	Cl	Cl	S	Me
11	Cl	H	Cl	S	Me
12	H	H	F	S	Me
13	H	H	CF_3	S	Cl
14	H	Cl	Cl	S	Cl
15	Cl	H	Cl	S	Cl
16	H	H	H	O	Me
17	H	Cl	H	O	Me
18	H	H	CF_3	O	Me
19	H	CF_3	H	O	Me
20	F	H	H	O	Me
21	Cl	Cl	H	O	Me
22	H	H	Me	O	Me
23	H	F	H	O	Me
24	Cl	H	H	O	Me
25	H	Cl	Cl	O	Me
26	Cl	H	Cl	O	Me
27	H	H	F	O	Me
28	H	H	CF_3	O	Cl
29	H	Cl	Cl	O	Cl
30	Cl	H	Cl	O	Cl

The biological activities studied here are the *in vitro* cell growth inhibition of human colorectal (SW620 and HT29) and human gastric (MGC803 and MKN45) cancer cell lines by the aforementioned molecules [5]. The activities are shown in Table 2.

Table 2. Biological activities of *N*-3-benzimidazolephenylbisamide derivatives

Mol.	log(IC_{50}) SW620	log(IC_{50}) HT29	log(IC_{50}) MGC803	log(IC_{50}) MKN45
1	1.83	1.46	1.78	1.76
2	----	1.55	1.71	1.64
3	1.86	1.24	0.81	1.01
4	1.19	0.91	0.72	0.78
5	0.81	0.27	0.49	0.38
6	----	1.80	----	----
7	1.78	1.15	0.70	1.05
8	----	1.74	----	1.94
9	1.76	1.37	1.65	1.71
10	1.49	0.80	0.81	0.92
11	1.76	1.06	0.54	0.72
12	1.61	0.28	0.45	0.63
13	1.81	1.11	0.73	0.89
14	1.40	0.69	0.71	0.66
15	1.70	0.78	0.48	0.57
16	1.48	1.21	1.60	1.55
17	1.20	1.19	1.32	1.45
18	1.18	0.89	1.17	1.43
19	0.98	0.55	1.12	0.98
20	0.61	-0.12	0.40	0.26
21	1.62	1.69	----	1.94
22	1.42	0.71	----	0.80
23	1.60	1.58	1.65	1.72
24	1.55	0.95	1.29	1.33
25	0.79	0.01	0.78	0.76
26	1.09	0.42	0.44	0.41
27	1.55	-0.01	-0.80	-0.62
28	0.47	-0.23	-0.92	-0.06
29	1.36	0.47	0.59	0.50
30	1.53	-0.14	-1.21	-0.46

Calculation of the electronic structure

We worked with the common skeleton hypothesis affirming that there is a set of atoms, shared with all the molecules analyzed, that explains nearly all the biological activities. The effect of the substituents is to modify the electronic structure of this common skeleton and/or influencing the correct placement of the drug. The common skeleton is presented in Fig. 2, together with the atom numbering used in the resulting statistical equations.

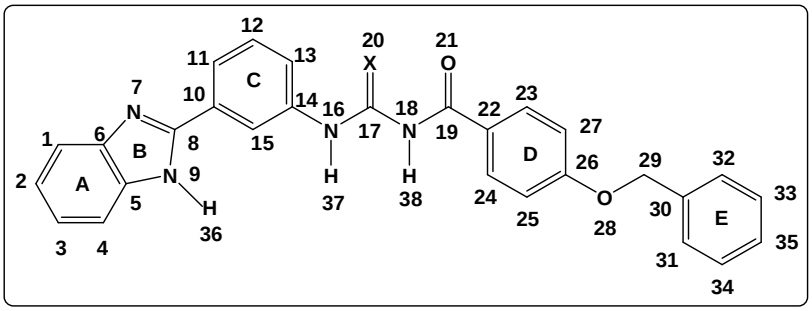

Figure 2. Common skeleton numbering

Molecular geometries were fully optimized at the B3LYP/6-31G(d,p) level of theory with the Gaussian package [70]. From the corrected Mulliken Population Analysis result we obtained numerical values for all electronic local atomic reactivity indices [71, 72]. The D-CENT-QSAR software was used [73]. Since the system of linear equations cannot be solved because the number of molecules is smaller than the number of unknown coefficients, a linear multiple regression analysis (LMRA) was carried out. The Statistica software was used [74].

RESULTS

HT-29 RESULTS

After finding and deleting the outliers we obtained the following equation:

$$\log(IC_{50}) = -2.02 - 0.88\eta_{14} + 0.029S_{33}^{N}(LUMO)^{*} - 0.58S_{35}^{E} - 1.60Q_{32} - \\ -0.01S_{4}^{N}(LUMO+2)^{*} - 0.41\mu_{19} - 0.008S_{1}^{N}(LUMO+1)^{*} \quad (1)$$

with n=28, R= 0.98, R^2= 0.97, adj-R^2= 0.92, F(7,20)=82.84 (p<0.000001) and a standard error of estimate of 0.12. No outliers were detected and no residuals fall outside the ±2σ limits. Here, η_{14} is the local atomic hardness of atom 14, $S_{33}^{N}(LUMO)^{*}$ is the nucleophilic superdelocalizabity of the lowest vacant MO localized on atom 33, S_{35}^{E} is the total atomic electrophilic superdelocalizability of atom 35, Q_{32} is the net charge of atom 32, $S_{4}^{N}(LUMO+2)^{*}$ is the nucleophilic superdelocalizability of the third lowest vacant MO localized on atom 4, μ_{19} is the local atomic electronic chemical potential of atom 19 and $S_{1}^{N}(LUMO+1)^{*}$ is the nucleophilic superdelocalizability of the second lowest vacant MO localized on atom 1. Table 3 shows the beta coefficients and the results of the t-test for significance of coefficients of Eq. 1. Table 4 displays the squared correlation coefficients for the variables appearing in Eq. 1, showing that there are no significant internal correlations. Fig. 3 displays the plot of observed *vs.* calculated log (IC_{50}) values. The associated statistical parameters of Eq. 1 indicate that this equation is statistically significant and that the variation of the numerical value of a group of seven local atomic reactivity indices of atoms of the common skeleton explains about 92% of the variation of the *in vitro* cell growth inhibition of human colorectal HT29 cancer cell line.

Table 3. Beta coefficients and *t*-test for significance of the coefficients in Eq. 1

	Beta	t(20)	p-level
η_{14}	-0.42	-9.42	<0.000001
$S_{33}^{N}(LUMO)^{*}$	0.29	5.18	<0.00004
S_{35}^{E}	-0.53	-11.36	<0.000001
Q_{32}	-0.39	-6.86	<0.000001
$S_{4}^{N}(LUMO+2)^{*}$	-0.31	-6.00	<0.000007
μ_{19}	-0.19	-3.85	<0.001
$S_{1}^{N}(LUMO+1)^{*}$	-0.17	-3.48	<0.002

Table 4. Squared correlation coefficients for the variables appearing in Eq. 1

	η_{14}	$S_{33}^{N}(LUMO)^{*}$	S_{35}^{E}	Q_{32}	$S_{4}^{N}(LUMO+2)^{*}$	μ_{19}
$S_{33}^{N}(LUMO)^{*}$	0.006	1				
S_{35}^{E}	0.008	0.03	1			
Q_{32}	0.02	0.3	0.04	1		
$S_{4}^{N}(LUMO+2)^{*}$	0.04	0.03	0.002	0.05	1	
μ_{19}	0.01	0.003	0.1	0.06	0.03	1
$S_{1}^{N}(LUMO+1)^{*}$	0.08	0.006	0.005	0.04	0.3	0.0004

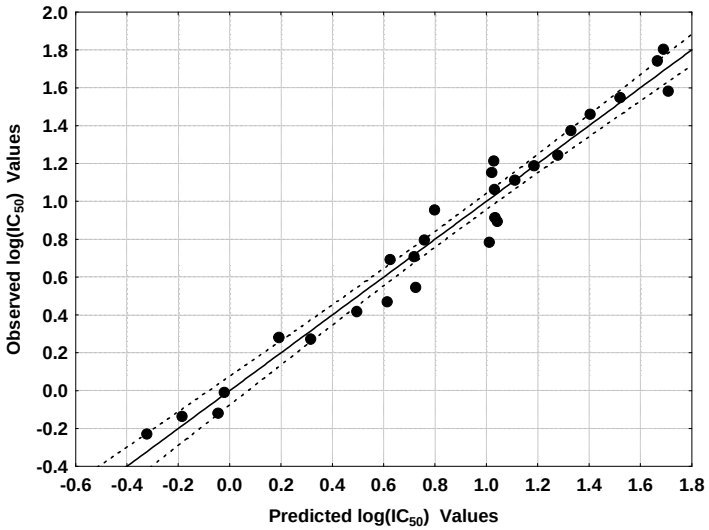

Figure 3. Observed *versus* calculated values (Eq. 1) of log (IC_{50}). Dashed lines denote the 95% confidence interval

MGC803 RESULTS

After finding and deleting the outliers we found the following equation:

$$\log(IC_{50}) = -12.72 - 1.03S_{35}^{E} + 0.02S_{25}^{N}(LUMO+2)^{*} + 0.71S_{15}^{E}(HOMO-1)^{*} + \\ +0.04S_{18}^{N}(LUMO+1)^{*} - 0.57S_{32}^{E} + 0.15S_{23}^{N}(LUMO+1)^{*} + 0.27S_{24}^{E}(HOMO-1)^{*} \quad (2)$$

with n=25, R= 0.98, R^2= 0.97, adj-R^2= 0.96, F(7,17)=78.04 (p<0.000001) and a standard error of estimate of 0.16. No outliers were detected and no residuals fall outside the ±2σ limits. Here, S_{35}^{E} is the total atomic electrophilic superdelocalizability of atom 35, $S_{25}^{N}(LUMO+2)^{*}$ is the nucleophilic superdelocalizability of the third lowest vacant MO localized on atom 25, $S_{15}^{E}(HOMO-1)^{*}$ is the electrophilic superdelocalizability of the second highest occupied MO localized on atom 15, $S_{18}^{N}(LUMO+1)^{*}$ is the nucleophilic superdelocalizability of the second lowest vacant MO localized on atom 18, S_{32}^{E} is the total atomic electrophilic superdelocalizability of atom 32, $S_{23}^{N}(LUMO+1)^{*}$ is the nucleophilic superdelocalizability of the second lowest vacant MO localized on atom 23 and $S_{24}^{E}(HOMO-1)^{*}$ is the electrophilic superdelocalizability of the second highest occupied MO localized on atom 24. Table 5 shows the beta coefficients and the results of the t-test for significance of coefficients of Eq. 2. Table 6 displays the squared correlation coefficients for the variables appearing in Eq. 2, showing that there are no significant internal correlations. Fig. 4 displays the plot of observed *vs.* calculated log (IC_{50}) values. The associated statistical parameters of Eq. 2 indicate that this equation is statistically significant and that the variation of the numerical value of a group of seven local atomic reactivity indices of atoms of the common skeleton explains about 96% of the variation of the *in vitro* cell growth inhibition of the human colorectal MGC803 cancer cell line.

Table 5. Beta coefficients and *t*-test for significance of the coefficients in Eq. 2

	Beta	t(17)	p-level
S_{35}^{E}	-0.73	-15.92	<0.000001
$S_{25}^{N}(LUMO+2)^{*}$	0.27	6.21	<0.00001
$S_{15}^{E}(HOMO-1)^{*}$	0.42	7.16	<0.000001
$S_{18}^{N}(LUMO+1)^{*}$	0.21	3.86	<0.001
S_{32}^{E}	-0.43	-9.45	<0.000001
$S_{23}^{N}(LUMO+1)^{*}$	0.19	3.14	<0.006
$S_{24}^{E}(HOMO-1)^{*}$	0.13	2.75	<0.01

Table 6. Squared correlation coefficients for the variables appearing in Eq. 2

	S_{35}^{E}	$S_{25}^{N}(LUMO+2)*$	$S_{15}^{E}(HOMO-1)*$	$S_{18}^{N}(LUMO+1)*$	S_{32}^{E}	$S_{23}^{N}(LUMO+1)*$
$S_{25}^{N}(LUMO+2)*$	0	1				
$S_{15}^{E}(HOMO-1)*$	0.003	0.04	1			
$S_{18}^{N}(LUMO+1)*$	0.06	0.03	0.1	1		
S_{32}^{E}	0.008	0.0001	0.006	0.06	1	
$S_{23}^{N}(LUMO+1)*$	0.008	0.0004	0.4	0.10	0.003	1
$S_{24}^{E}(HOMO-1)*$	0.0004	0.0004	0	0.06	0.01	0.02

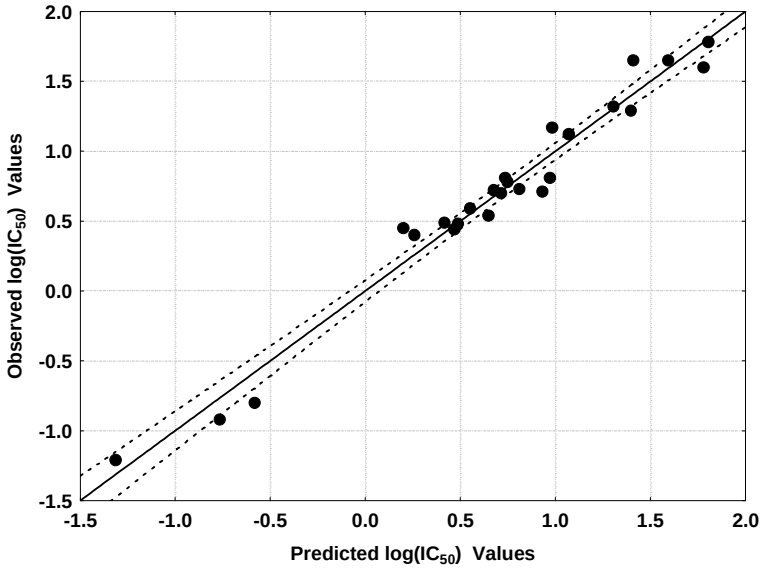

Figure 4. Observed *versus* calculated values (Eq. 2) of log (IC_{50}). Dashed lines denote the 95% confidence interval

MKN45 RESULTS

After finding and deleting the outliers we obtained the following equation:

$$\log(IC_{50}) = -6.68 - 0.21S_{13}^{N}(LUMO+1)* - 0.75S_{35}^{E} + 0.03S_{27}^{N}(LUMO+2)* + \\ +0.24S_{25}^{E}(HOMO-1)* + 0.29S_{24}^{E}(HOMO-1)* - 0.009S_{31}^{N}(LUMO+1)* + \\ +0.0009S_{11}^{N}(LUMO+2)* + 0.22S_{21}^{E}(HOMO-1)* \qquad (3)$$

with n=23, R= 0.99, R^2= 0.98, adj-R^2= 0.98, F(8,14)=78.04 (p<0.000001) and a standard error of estimate of 0.10. No outliers were detected and no residuals fall outside the ±2σ limits. Here, $S_{13}^{N}(LUMO+1)*$ is the nucleophilic superdelocalizability of the second lowest vacant MO localized on atom 13, S_{35}^{E} is the total atomic electrophilic superdelocalizability of atom 35, $S_{27}^{N}(LUMO+2)*$ is the nucleophilic superdelocalizability of the third lowest vacant MO localized on atom 27, $S_{25}^{E}(HOMO-1)*$ is the electrophilic superdelocalizability of the second highest occupied MO localized on atom 25, $S_{24}^{E}(HOMO-1)*$ is the electrophilic superdelocalizability of the second highest occupied MO localized on atom 24, $S_{31}^{N}(LUMO+1)*$ is the nucleophilic superdelocalizability of the second lowest vacant MO localized on atom 31, $S_{11}^{N}(LUMO+2)*$ is the nucleophilic superdelocalizability of the third lowest vacant MO localized on atom 11 and $S_{21}^{E}(HOMO-1)*$ is the electrophilic superdelocalizability

of the second highest occupied MO localized on atom 21. Table 7 shows the beta coefficients and the results of the t-test for significance of coefficients of Eq. 3. Table 8 displays the squared correlation coefficients for the variables appearing in Eq. 3, showing that there are no significant internal correlations. Fig. 5 displays the plot of observed *vs.* calculated log (IC_{50}) values. The associated statistical parameters of Eq. 1 indicate that this equation is statistically significant and that the variation of the numerical value of a group of eight local atomic reactivity indices of atoms of the common skeleton explains about 98% of the variation of the *in vitro* cell growth inhibition of the human colorectal MKN45 cancer cell line.

Table 7. Beta coefficients and *t*-test for significance of the coefficients in Eq. 3

	Beta	t(14)	p-level
$S_{13}^{N}(LUMO+1)^*$	-0.56	-13.92	<0.000001
S_{35}^{E}	-0.62	-16.40	<0.000001
$S_{27}^{N}(LUMO+2)^*$	0.31	7.20	<0.000005
$S_{25}^{E}(HOMO-1)^*$	0.22	5.16	<0.0001
$S_{24}^{E}(HOMO-1)^*$	0.18	4.71	<0.0003
$S_{31}^{N}(LUMO+1)^*$	-0.13	-3.47	<0.004
$S_{11}^{N}(LUMO+2)^*$	0.14	3.17	<0.007
$S_{21}^{E}(HOMO-1)^*$	0.11	2.69	<0.02

Table 8. Squared correlation coefficients for the variables appearing in Eq. 3

	$S_{13}^{N}(LUMO+1)^*$	S_{35}^{E}	$S_{27}^{N}(LUMO+2)^*$	$S_{25}^{E}(HOMO-1)^*$	$S_{24}^{E}(HOMO-1)^*$	$S_{31}^{N}(LUMO+1)^*$	$S_{11}^{N}(LUMO+2)^*$
S_{35}^{E}	0.29	1.00					
$S_{27}^{N}(LUMO+2)^*$	0.08	1					
$S_{25}^{E}(HOMO-1)^*$	0.07	0.01	1				
$S_{24}^{E}(HOMO-1)^*$	0.02	0.07	0.07	1			
$S_{31}^{N}(LUMO+1)^*$	0.08	0.001	0.08	0.005	1		
$S_{11}^{N}(LUMO+2)^*$	0.004	0.04	0.004	0.04	0.04	1	
$S_{21}^{E}(HOMO-1)^*$	0.005	0.07	0.3	0.2	0.02	0.005	1

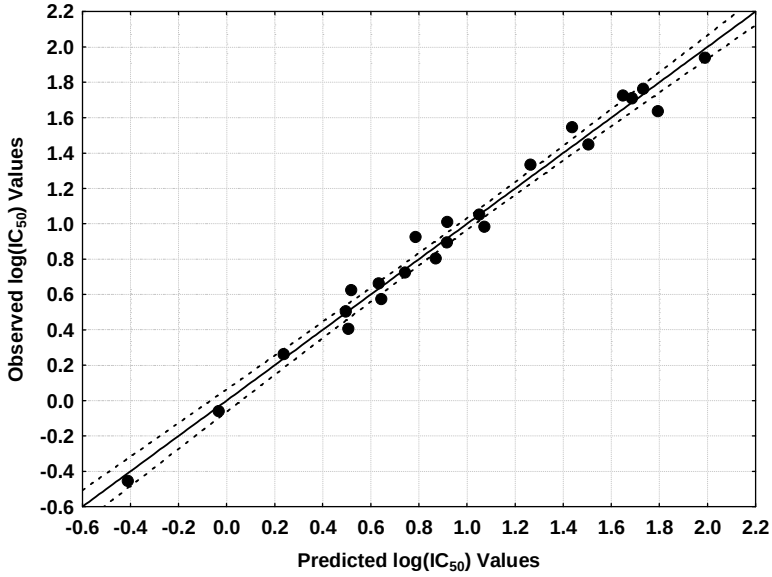

Figure 5. Observed *versus* calculated values (Eq. 3) of log (IC_{50}). Dashed lines denote the 95% confidence interval

SW620 RESULTS

After detecting and deleting the outliers we found the following equation:

$$\log(IC_{50}) = 2.89 - 1.46Q_{32} - 0.09S_{17}^{N}(LUMO)^{*} + 0.45\mu_{34} + 0.24S_{12}^{E}(HOMO-2)^{*} - \\ -0.37F_{31}(LUMO)^{*} + 0.34F_{32}(LUMO)^{*} \quad (4)$$

with n=24, R= 0.97, R^2= 0.95, adj-R^2= 0.93, F(6,17)=50.85 (p<0.000001) and a standard error of estimate of 0.10. No outliers were detected and no residuals fall outside the ±2σ limits. Here, Q_{32} is the net charge of atom 32, $S_{17}^{N}(LUMO)^{*}$ is the nucleophilic superdelocalizability of the lowest vacant MO localized on atom 17, μ_{34} is the local atomic electronic chemical potential of atom 34, $S_{12}^{E}(HOMO-2)^{*}$ is the electrophilic superdelocalizability of the third highest occupied MO localized on atom 12, $F_{31}(LUMO)^{*}$ is the Fukui index of the lowest vacant MO localized on atom 31 and $F_{32}(LUMO)^{*}$ is the Fukui index of the lowest vacant MO localized on atom 32. Table 9 shows the beta coefficients and the results of the t-test for significance of coefficients of Eq. 4. Table 10 displays the squared correlation coefficients for the variables appearing in Eq. 4, showing that there are no significant internal correlations. Fig. 6 displays the plot of observed *vs.* calculated log (IC_{50}) values. The associated statistical parameters of Eq. 4 indicate that this equation is statistically significant and that the variation of the numerical value of a group of six local atomic reactivity indices of atoms of the common skeleton explains about 93% of the variation of the *in vitro* cell growth inhibition of the human colorectal SW620 cancer cell line.

Table 9. Beta coefficients and *t*-test for significance of the coefficients in Eq. 4

	Beta	t(17)	p-level
Q_{32}	-0.58	-8.91	<0.000001
$S_{17}^{N}(LUMO)^{*}$	-0.46	-7.49	<0.000001
μ_{34}	0.28	4.42	<0.0004
$S_{12}^{E}(HOMO-2)^{*}$	0.20	3.13	<0.006
$F_{31}(LUMO)^{*}$	-0.19	-2.93	<0.009
$F_{32}(LUMO)^{*}$	0.13	2.23	<0.04

Table 10. Squared correlation coefficients for the variables appearing in Eq. 4

	Q_{32}	$S_{17}^{N}(LUMO)^{*}$	μ_{34}	$S_{12}^{E}(HOMO-2)^{*}$	$F_{31}(LUMO)^{*}$
$S_{17}^{N}(LUMO)^{*}$	0.04	1			
μ_{34}	0.03	0.08	1		
$S_{12}^{E}(HOMO-2)^{*}$	0.03	0.1	0.08	1	
$F_{31}(LUMO)^{*}$	0.1	0.0009	0.07	0.02	1
$F_{32}(LUMO)^{*}$	0.06	0.0064	0.002	0.008	0.02

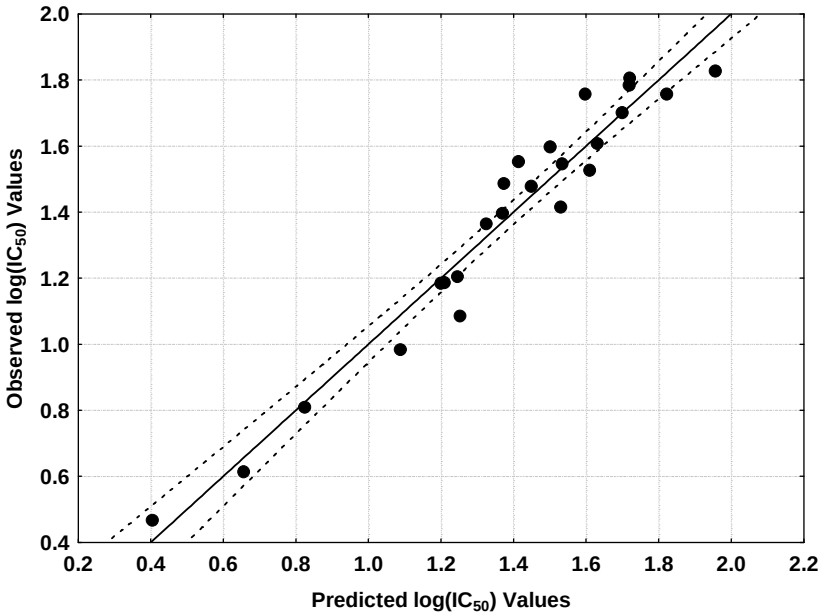

Figure 6. Observed versus calculated values (Eq. 4) of log (IC_{50}). Dashed lines denote the 95% confidence interval

Local Molecular Orbitals

Tables 11-16 display the local molecular orbital structure of atoms appearing in Eqs. 1-4 [37, 38].

Table 11. Local molecular orbital structure of atoms 1, 4 and 11

Mol	Atom 1 (C)	Atom 4 (C)	Atom 11 (C)
1 (129)	126π127π128π-131π136π137π	126π127π128π-131π136π137π	124π127π128π-130π131π132π
2 (137)	134π135π137π-139π143π144π	134π135π137π-139π143π144π	135π136π137π-138π139π143π
3 (145)	142π143π145π-148π151π152π	142π143π145π-148π151π152π	143π144π145π-146π148π151π
4 (145)	142π143π145π-148π151π152π	142π143π145π-148π151π152π	143π144π145π-146π148π151π
5 (133)	130π131π133π-135π138π140π	130π131π133π-135π138π140π	131π132π133π-134π135π137π
6 (145)	142π143π145π-148π149π151π	142π143π145π-148π149π151π	143π144π145π-146π148π151π
7 (133)	130π131π133π-135π140π141π	130π131π133π-135π140π141π	131π132π133π-134π135π136π
8 (133)	130π131π133π-135π140π141π	130π131π133π-135π140π141π	131π132π133π-134π135π137π
9 (137)	134π135π136π-138π139π144π	134π135π136π-139π144π145π	133π135π136π-138π139π142π
10 (145)	142π143π144π-147π153π155π	142π143π144π-147π153π155π	141π143π144π-146π147π150π
11 (145)	142π143π144π-147π153π155π	142π143π144π-147π153π155π	141π143π144π-146π147π150π
12 (133)	130π131π132π-135π140π142π	130π131π132π-135π140π142π	129π131π132π-134π135π136π
13 (149)	147π148π149π-150π151π156π	146π147π148π-151π156π157π	146π147π148π-150π151π153π
14 (149)	146π147π148π-150π151π157π	146π147π148π-151π157π159π	146π147π148π-150π151π153π
15 (149)	147π148π149π-150π151π156π	146π147π148π-151π156π158π	144π147π148π-150π151π154π
16 (125)	123π124π125π-126π127π132π	123π124π125π-126π127π132π	123π124π125π-126π127π131π
17 (133)	131π132π133π-134π135π140π	131π132π133π-135π140π143π	131π132π133π-134π135π139π
18 (141)	139π140π141π-143π148π150π	139π140π141π-143π148π150π	139π140π141π-142π143π147π
19 (141)	139π140π141π-143π148π149π	139π140π141π-143π148π149π	139π140π141π-142π143π147π
20 (129)	127π128π129π-130π131π136π	127π128π129π-130π131π136π	127π128π129π-130π131π135π
21 (141)	139π140π141π-142π143π149π	139π140π141π-143π149π151π	139π140π141π-142π143π148π
22 (129)	127π128π129π-130π131π136π	127π128π129π-130π131π136π	127π128π129π-130π131π135π
23 (129)	127π128π129π-130π131π136π	127π128π129π-131π136π138π	127π128π129π-130π131π134π
24 (133)	131π132π133π-134π135π140π	131π132π133π-134π135π140π	131π132π133π-134π135π139π
25 (141)	139π140π141π-142π143π149π	139π140π141π-143π149π151π	139π140π141π-142π143π148π
26 (141)	139π140π141π-144π145π149π	139π140π141π-144π145π149π	139π140π141π-142π144π147π
27 (129)	127π128π129π-130π131π136π	127π128π129π-131π136π137π	127π128π129π-130π131π135π
28 (133)	127π132π133π-134π135π140π	127π132π133π-134π135π140π	131π132π133π-134π135π137π
29 (133)	126π132π133π-134π135π140π	126π132π133π-134π135π140π	131π132π133π-134π135π137π
30 (133)	127π132π133π-134π135π140π	127π132π133π-134π135π140π	131π132π133π-134π135π137π

Table 12. Local molecular orbital structure of atoms 12, 13 and 15

Mol	Atom 12 (C)	Atom 13 (C)	Atom 15 (C)
1 (129)	124π127π129π-131π132π133π	124π127π128π-130π131π136π	127π128π129π-130π131π132π
2 (137)	133π135π136π-139π141π142π	135π136π137π-138π139π144π	135π136π137π-138π139π141π
3 (145)	141π143π144π-148π149π151π	143π144π145π-146π148π152π	143π144π145π-146π148π149π
4 (145)	141π143π144π-148π150π151π	143π144π145π-146π148π152π	143π144π145π-146π148π150π
5 (133)	129π131π132π-135π137π138π	126π132π133π-134π135π140π	131π132π133π-134π135π137π
6 (145)	141π143π144π-148π150π151π	143π144π145π-146π148π149π	143π144π145π-146π148π149π
7 (133)	129π131π132π-135π136π138π	131π132π133π-134π135π140π	131π132π133π-134π135π136π
8 (133)	129π131π132π-135π137π138π	131π132π133π-134π135π140π	131π132π133π-134π135π137π
9 (137)	132π135π137π-139π141π142π	132π135π136π-138π139π144π	135π136π137π-138π139π141π
10 (145)	140π141π143π-147π150π151π	137π143π144π-146π147π153π	143π144π145π-146π147π148π
11 (145)	140π141π143π-147π150π151π	137π143π144π-146π147π153π	143π144π145π-147π148π150π
12 (133)	128π129π131π-135π136π137π	125π131π132π-134π135π140π	131π132π133π-135π136π137π
13 (149)	146π147π149π-151π153π156π	144π147π148π-150π151π156π	147π148π149π-151π152π153π
14 (149)	144π145π146π-151π152π153π	146π147π148π-150π151π157π	147π148π149π-151π152π153π
15 (149)	144π147π149π-151π154π156π	144π147π148π-150π151π156π	147π148π149π-151π153π154π
16 (125)	118π123π124π-127π131π132π	123π124π125π-126π127π131π	123π124π125π-127π131π132π
17 (133)	131π132π133π-135π139π140π	131π132π133π-134π135π139π	131π132π133π-135π139π140π
18 (141)	139π140π141π-143π147π148π	139π140π141π-142π143π147π	139π140π141π-143π147π148π
19 (141)	136π139π140π-143π147π148π	139π140π141π-142π143π147π	139π140π141π-143π147π148π
20 (129)	127π128π129π-131π135π136π	127π128π129π-130π131π135π	127π128π129π-131π135π136π
21 (141)	139π140π141π-143π148π149π	139π140π141π-142π143π148π	139π140π141π-143π148π149π
22 (129)	122π127π128π-131π135π136π	127π128π129π-130π131π135π	127π128π129π-131π135π136π
23 (129)	127π128π129π-131π134π135π	127π128π129π-130π131π135π	127π128π129π-131π134π135π
24 (133)	127π131π132π-135π139π140π	131π132π133π-134π135π139π	131π132π133π-135π139π140π
25 (141)	139π140π141π-143π148π149π	139π140π141π-142π143π148π	139π140π141π-143π148π149π
26 (141)	136π139π140π-144π145π147π	139π140π141π-142π144π145π	139π140π141π-144π145π147π
27 (129)	123π127π128π-131π135π136π	127π128π129π-130π131π135π	127π128π129π-131π135π136π
28 (133)	124π131π133π-134π135π137π	131π132π133π-134π135π138π	129π131π133π-134π135π137π
29 (133)	124π131π133π-134π135π137π	131π132π133π-134π135π137π	128π131π133π-134π135π137π
30 (133)	125π131π133π-135π137π138π	131π132π133π-134π135π138π	128π131π133π-134π135π137π

Table 13. Local molecular orbital structure of atoms 17, 18 and 21

Mol	Atom 17 (C)	Atom 18 (N)	Atom 21 (O)
1 (129)	124π127π129π-130π132π133π	125π127π129π-130π132π133π	127π128π129π-130π131π132π
2 (137)	133π135π136π-138π139π141π	133π135σ136σ-138π139π141π	130π132π133π-138π145π148π
3 (145)	141π143π144π-146π148π149π	141π143σ144σ-146π148π151π	139π140π141π-146π153π155π
4 (145)	141π143π144π-146π148π150π	141π143σ144σ-146π148π150π	135π139π140π-146π153π155π
5 (133)	129π131π132π-134π135π137π	129π131σ132σ-134π135π137π	122π126π128π-134π141π143π
6 (145)	141π143π144π-146π148π150π	141π143σ144σ-146π148π151π	139π140π141π-146π154π157π
7 (133)	129π131π132π-134π136π138π	129π131σ132σ-134π135π136π	126π128π129π-134π141π143π
8 (133)	129π131π132π-134π135π137π	129π131σ132σ-134π135π137π	123π126π128π-134π141π143π
9 (137)	132π135π137π-138π139π141π	133π135σ137σ-138π142π144π	133π135π137π-138π139π142π
10 (145)	141π143π145π-146π148π149π	140π141π145σ-150π151π154π	139π140π145π-146π147π158π
11 (145)	141π143π145π-146π148π150π	140π141π145σ-150π151π154π	139π140π145π-146π147π150π
12 (133)	129π131π133π-134π136π137π	128π129π133σ-136π137π138π	128π129π133π-134π135π136π
13 (149)	147π148π149π-150π151π152π	146π147π149σ-150π153π156π	147π148π149π-150π151π153π
14 (149)	145π146π149π-150π152π153π	144π145π149σ-153π154π155π	144π145π149π-150π151π154π
15 (149)	147π148π149π-150π151π153π	146π147π149σ-150π154π156π	147π148π149π-150π151π154π
16 (125)	115π121π123π-126π131π132π	116π121σ123π-126π131π137π	121π122π123π-126π127π134π
17 (133)	123π129π131π-134π139π140π	129σ130π131π-134π139π145π	129π130π131π-134π135π144π
18 (141)	131π137π139π-142π147π148π	137σ138π139π-142π147π153π	137π138π139π-142π143π144π
19 (141)	131π137π139π-142π147π148π	134π137σ139π-142π147π153π	137π138π139π-142π143π150π
20 (129)	119π125π127π-130π135π136π	125σ127π128π-130π131π135π	125π126π127π-130π131π139π
21 (141)	131π137π139π-142π148π149π	132π137π139σ-142π148π155π	137π138π139π-142π143π144π
22 (129)	119π124π127π-130π135π136π	120π124σ127π-130π131π135π	125π126π127π-130π131π138π
23 (129)	119π125π127π-130π134π135π	120π125σ127π-130π135π141π	125π126π127π-130π131π139π
24 (133)	123π129π131π-134π139π140π	125π129σ131π-134π135π139π	129π130π131π-134π135π143π
25 (141)	131π137π139π-142π148π149π	132π137σ139π-142π148π155π	137π138π139π-142π143π144π
26 (141)	131π137π139π-142π147π149π	133π137σ139π-142π147π155π	137π138π139π-142π145π151π
27 (129)	119π125π127π-130π135π136π	121π125σ127π-130π135π141π	125π126π127π-130π131π138π
28 (133)	123π129π131π-134π135π137π	125π129σ131π-135π138π144π	129π130π131π-134π135π144π
29 (133)	123π128π131π-134π135π137π	125π128σ131π-135π137π144π	129π130π131π-134π135π143π
30 (133)	123π128π131π-134π135π137π	125π128σ131π-134π135π138π	129π130π131π-134π135π143π

Table 14. Local molecular orbital structure of atoms 23, 24 and 25

Mol	Atom 23 (C)	Atom 24 (C)	Atom 25 (C)
1 (129)	119π120π125π-130π131π133π	119π120π125π-130π131π132π	119π124π125π-130π132π133π
2 (137)	127π132π133π-138π139π140π	127π128π133π-138π139π140π	127π132π133π-138π140π141π
3 (145)	135π140π141π-146π147π149π	135π137π141π-146π147π148π	135π140π141π-146π147π149π
4 (145)	135π140π141π-146π149π150π	135π137π141π-146π148π149π	135π140π141π-146π147π149π
5 (133)	124π128π129π-134π135π137π	123π124π129π-134π135π137π	124π128π129π-134π137π138π
6 (145)	136π140π141π-146π150π151π	135π136π141π-146π148π150π	136π140π141π-146π150π151π
7 (133)	123π128π129π-134π135π136π	122π123π129π-134π135π136π	123π128π129π-134π136π138π
8 (133)	123π128π129π-134π135π136π	123π124π129π-134π135π136π	123π128π129π-134π136π137π
9 (137)	128π129π133π-138π139π141π	128π129π133π-138π139π142π	128π129π133π-142π143π150π
10 (145)	136π140π141π-146π147π148π	134π135π141π-146π147π148π	139π140π141π-146π148π149π
11 (145)	136π140π141π-146π147π149π	135π136π141π-146π147π148π	136π140π141π-146π148π149π
12 (133)	127π128π129π-134π135π136π	122π123π129π-134π135π136π	127π128π129π-134π136π137π
13 (149)	139π141π145π-150π151π152π	141π143π145π-150π151π152π	141π143π145π-152π153π155π
14 (149)	143π144π145π-150π151π152π	139π140π145π-150π151π152π	143π144π145π-150π152π153π
15 (149)	140π142π145π-150π151π154π	140π142π145π-150π151π154π	140π142π145π-154π155π162π
16 (125)	116π121π122π-126π127π128π	120π121π122π-126π127π128π	114π116π122π-126π128π129π
17 (133)	125π129π130π-134π135π136π	125π129π130π-134π135π136π	125π128π130π-134π136π137π
18 (141)	134π137π138π-142π143π145π	134π137π138π-142π143π144π	132π133π138π-142π144π145π
19 (141)	134π137π138π-142π143π145π	134π137π138π-142π143π145π	133π134π138π-142π145π146π
20 (129)	120π125π126π-130π131π132π	122π125π126π-130π131π132π	118π120π126π-130π132π133π
21 (141)	132π137π138π-142π143π145π	133π137π138π-142π143π144π	130π132π138π-142π144π145π
22 (129)	120π124π126π-130π131π132π	120π124π126π-130π131π132π	118π120π126π-130π132π133π
23 (129)	122π125π126π-130π131π132π	122π125π126π-130π131π132π	120π124π126π-130π132π133π
24 (133)	125π129π130π-134π135π138π	125π129π130π-134π135π138π	122π125π130π-134π138π143π
25 (141)	132π137π138π-142π143π145π	133π137π138π-142π143π144π	130π132π138π-142π144π145π
26 (141)	133π137π138π-142π145π146π	133π137π138π-142π145π146π	130π133π138π-142π146π151π
27 (129)	121π125π126π-130π131π133π	121π125π126π-130π131π132π	118π121π126π-130π132π133π
28 (133)	125π129π130π-134π135π136π	126π129π130π-134π135π136π	122π125π130π-135π136π137π
29 (133)	128π129π130π-134π135π136π	128π129π130π-134π135π136π	125π129π130π-135π136π137π
30 (133)	125π128π130π-134π135π136π	128π129π130π-134π135π136π	125π129π130π-134π135π136π

Table 15. Local molecular orbital structure of atoms 27, 31 and 32

Mol	Atom 27 (C)	Atom 31 (C)	Atom 32 (C)
1 (129)	119π120π125π-132π133π134π	115π122π123π-133π134π135π	115π122π123π-133π134π135π
2 (137)	128π132π133π-140π141π142π	122π131π132π-140π142π143π	123π128π131π-140π141π142π
3 (145)	137π140π141π-147π148π149π	130π136π137π-147π150π161π	125π136π137π-147π150π160π
4 (145)	137π140π141π-149π150π153π	130π136π137π-147π149π161π	125π136π137π-147π149π150π
5 (133)	124π128π129π-137π138π141π	123π124π127π-136π138π139π	113π117π127π-136π138π139π
6 (145)	136π140π141π-150π154π157π	135π136π138π-147π148π149π	135π136π138π-147π148π149π
7 (133)	123π128π129π-136π138π141π	125π126π127π-137π138π139π	125π126π127π-137π138π139π
8 (133)	124π128π129π-136π137π138π	124π127π128π-136π137π139π	117π124π127π-136π137π138π
9 (137)	129π130π133π-143π144π148π	123π126π131π-140π141π142π	122π123π131π-140π141π142π
10 (145)	139π140π141π-146π148π149π	136π139π140π-148π149π151π	130π131π136π-148π149π150π
11 (145)	139π140π141π-149π150π151π	130π135π139π-147π148π149π	131π135π139π-148π149π150π
12 (133)	122π127π129π-136π137π138π	124π127π128π-137π138π139π	124π127π128π-136π137π138π
13 (149)	140π141π145π-153π155π156π	140π141π143π-152π153π154π	140π141π143π-152π154π155π
14 (149)	139π143π145π-153π154π155π	143π144π145π-152π153π154π	133π135π141π-152π153π154π
15 (149)	140π142π145π-154π155π156π	132π133π139π-152π153π154π	135π139π143π-152π153π154π
16 (125)	120π121π122π-126π128π129π	111π119π120π-128π129π130π	111π119π120π-128π129π130π
17 (133)	125π128π130π-134π136π137π	125π128π130π-136π137π138π	124π125π128π-136π137π138π
18 (141)	133π134π138π-142π144π145π	132π133π134π-142π144π145π	132π133π134π-144π145π146π
19 (141)	134π137π138π-142π145π146π	132π133π134π-144π145π157π	132π133π134π-144π145π146π
20 (129)	120π122π126π-130π132π133π	121π122π124π-132π133π134π	114π122π124π-132π133π134π
21 (141)	132π133π138π-142π144π145π	125π133π136π-142π143π144π	128π133π136π-144π145π146π
22 (129)	120π124π126π-130π132π133π	115π123π125π-132π133π134π	115π123π125π-132π133π134π
23 (129)	122π124π126π-130π132π133π	122π124π126π-132π133π134π	120π122π124π-132π133π134π
24 (133)	125π129π130π-134π138π139π	119π124π128π-136π137π141π	118π119π128π-136π137π141π
25 (141)	132π133π138π-142π144π145π	125π133π136π-142π143π144π	128π133π136π-144π145π146π
26 (141)	133π137π138π-142π146π147π	125π126π132π-142π143π144π	127π132π135π-142π143π144π
27 (129)	121π125π126π-130π133π134π	115π120π124π-132π133π134π	113π120π124π-132π134π142π
28 (133)	125π126π130π-135π136π137π	117π126π128π-136π137π138π	117π126π128π-136π137π139π
29 (133)	125π129π130π-135π136π138π	127π129π130π-136π137π138π	127π129π130π-138π139π149π
30 (133)	125π129π130π-134π135π136π	126π129π130π-136π137π138π	118π126π129π-137π138π139π

Table 16. Local molecular orbital structure of atoms 33 and 34

Mol.	Atom 33 (C)	Atom 34
1 (129)	115π122π123π-133π135π143π	115π122π123π-133π134π135π
2 (137)	128π131π132π-140π142π143π	123π128π131π-140π141π142π
3 (145)	130π136π137π-147π149π150π	130π136π137π-147π150π151π
4 (145)	130π136π137π-147π149π161π	130π136π137π-147π149π150π
5 (133)	123π124π127π-136π138π139π	113π117π127π-136π138π139π
6 (145)	135π136π138π-147π148π149π	135π136π138π-147π148π149π
7 (133)	125π126π127π-137π138π139π	125π126π127π-137π138π139π
8 (133)	118π124π127π-136π137π139π	118π124π127π-136π137π138π
9 (137)	123π126π131π-140π141π142π	122π123π131π-140π141π142π
10 (145)	136π139π140π-148π149π151π	134π136π139π-148π149π150π
11 (145)	134π135π139π-147π148π149π	130π135π139π-148π149π150π
12 (133)	127π128π129π-137π138π139π	124π127π128π-136π137π138π
13 (149)	140π141π143π-152π153π154π	139π140π143π-152π154π155π
14 (149)	143π144π145π-152π153π154π	135π141π143π-152π153π154π
15 (149)	132π135π139π-152π153π154π	135π139π143π-152π153π154π
16 (125)	111π119π120π-128π129π130π	111π119π120π-128π129π130π
17 (133)	125π128π130π-136π137π138π	124π125π128π-136π137π138π
18 (141)	132π133π134π-142π144π145π	132π133π134π-144π145π146π
19 (141)	132π133π134π-144π145π157π	132π133π134π-144π145π146π
20 (129)	121π122π124π-132π133π134π	115π122π124π-132π133π134π
21 (141)	128π133π136π-142π143π144π	126π133π136π-144π145π146π
22 (129)	115π123π125π-132π133π134π	115π123π125π-132π133π134π
23 (129)	122π124π126π-132π133π134π	120π122π124π-132π133π134π
24 (133)	119π124π128π-136π137π141π	118π119π128π-136π137π149π
25 (141)	128π133π136π-142π143π144π	126π133π136π-144π145π146π
26 (141)	125π127π132π-142π143π144π	127π132π135π-142π143π144π
27 (129)	113π120π124π-132π133π134π	115π120π124π-132π134π142π
28 (133)	118π126π128π-136π137π138π	118π126π128π-136π137π139π
29 (133)	127π129π130π-136π137π138π	118π127π129π-138π139π148π
30 (133)	126π129π130π-136π137π138π	118π126π129π-137π138π139π

DISCUSSION

Discussion of HT-29 results

Beta values (Table 3) show that the importance of variables is $S_{35}^{E} > \eta_{14} > Q_{32} > S_{4}^{N}(LUMO+2)^{*} > S_{33}^{N}(LUMO)^{*} >> \mu_{19} > S_{1}^{N}(LUMO+1)^{*}$. Eq. 2 shows that a high antiproliferative capacity is associated with high numerical values of η_{14}, low negative numerical values of S_{35}^{E} and μ_{19}, and with a positive value of the net charge of atom 32. The nature of the contribution of the nucleophilic superdelocalizabilities will be discussed case by case. Table 17 shows the local molecular orbital structure of atoms 14 and 19 appearing only in Eq. 2.

Atom 14 is a carbon in ring C (Fig. 2). η_{14} is the local atomic hardness of atom 14 and corresponds to the $HOMO_{14}^{*}$-$LUMO_{14}^{*}$ gap. Therefore, high values for this local reactivity index are obtained by enlarging the mentioned gap. From a strict theoretical point of view, this enlarging can be obtained by shifting downwards the $HOMO_{14}^{*}$ associated eigenvalue, by shifting upwards the $LUMO_{14}^{*}$ associated eigenvalue or by a combination of both procedures. If we examine Table 17, we can observe that in all molecules the $LUMO_{14}^{*}$ corresponds to the molecule's LUMO. Table 17 shows also that in eight cases (molecules 9-12, 14 and 28-30) the local $HOMO_{14}^{*}$ does not coincide with the molecular HOMO. Therefore, and as a preliminary hypothesis, we suggest that a better activity can be obtained by shifting downwards the $HOMO_{14}^{*}$ associated eigenvalue. This procedure leads to a lesser reactive $HOMO_{14}^{*}$. If this is the case, then atom 14 should act as an electron acceptor center and interact with an electron donor center. Atom 33 is a carbon in ring E (Fig. 2). $LUMO_{33}^{*}$ is a π MO in all molecules (Table 16). If the numerical values of $S_{33}^{N}(LUMO)^{*}$ are positive, a low value is associated with high activity. This result is obtained by shifting upwards the $LUMO_{33}^{*}$ eigenvalue making the MO less reactive. For this reason, we suggest that atom 33 is interacting with an electron deficient center. Atom 35 is a carbon in ring E (Fig. 2). S_{35}^{E} is always a negative number. As small negative values of this index are associated with high inhibitory activity, atom 35 should behave as an electron acceptor and interact with an electron rich center. Atom 32 is a carbon in ring E (Fig. 2). A positive net charge on this atom is related with high activity, suggesting that atom 32 is engaged in an electrostatic interaction with a negatively charged site. Atom 4 is a carbon in ring A (Fig. 2). The three highest occupied and the three lowest vacant local MOs are of π nature (Table 11). If the numerical values of $S_{4}^{N}(LUMO+2)^{*}$ are

positive, a high inhibitory activity is associated with high values of this index. High values are obtained by shifting downwards the MO energy making this MO more reactive. We suggest then that atom 4 is interacting with an electron rich center though the first three lowest vacant MOs. Atom 19 is the underlined carbon of the NC(X)NC(O) moiety linking rings C and D (Fig. 2, X=O or S).

Table 17. Local molecular orbital structure of atoms 14 and 19

Mol.	Atom 14 (C)	Atom 19 (C)
1 (129)	127π128π129π-130π131π132π	118σ120σ**124σ**-130π131π132π
2 (137)	135π136π137π-138π139π141π	124π126σ**132π**-138π139π144π
3 (145)	143π144π145π-146π148π151π	132π134σ**140π**-146π148π152π
4 (145)	143π144π145π-146π148π151π	134σ140π**144σ**-146π148π151π
5 (133)	131π132π133π-134π135π137π	122σ128π**132σ**-134π135π138π
6 (145)	143π144π145π-146π148π151π	132π134σ**140π**-146π148π151π
7 (133)	131π132π133π-134π135π136π	122σ128π132σ-134π135π141π
8 (133)	131π132π133π-134π135π137π	122σ128π132σ-134π135π138π
9 (137)	133π135π**136π**-138π139π142π	124π125σ**129σ**-138π139π142π
10 (145)	142π143π**144π**-146π147π150π	130π132π**135σ**-146π147π151π
11 (145)	141π143π**144π**-146π147π150π	133π136σ140π-146π147π150π
12 (133)	129π131π**132π**-134π135π136π	120σ121π123σ-134π135π136π
13 (149)	147π148π149π-150π151π153π	139σ141σ143σ-150π151π153π
14 (149)	145π146π**147π**-150π151π153π	132σ136π140σ-150π151π154π
15 (149)	147π148π149π-150π151π154π	137π140σ142σ-150π151π154π
16 (125)	123π124π125π-126π127π131π	114σ115π121σ-126π127π134π
17 (133)	131π132π133π-134π135π139π	122π123σ129σ-134π135π143π
18 (141)	139π140π141π-142π143π147π	130σ131σ137σ-142π143π144π
19 (141)	139π140π141π-142π143π147π	130π131σ137σ-142π143π149π
20 (129)	127π128π129π-130π131π135π	118π119σ125σ-130π131π132π
21 (141)	139π140π141π-142π143π148π	130π131σ137σ-142π143π144π
22 (129)	127π128π129π-130π131π135π	118σ119σ124σ-130π131π138π
23 (129)	127π128π129π-130π131π134π	118σ119σ125σ-130π131π138π
24 (133)	131π132π133π-134π135π139π	122σ123σ129σ-134π135π143π
25 (141)	139π140π141π-142π143π148π	130π131σ137σ-142π143π144π
26 (141)	139π140π141π-142π144π147π	130σ131σ137σ-142π144π145π
27 (129)	127π128π129π-130π131π135π	118σ119σ125σ-130π131π138π
28 (133)	120π131π**132π**-134π137π138π	122π123σ129σ-134π135π143π
29 (133)	120π131π**132π**-134π137π138π	122π123σ128σ-134π135π143π
30 (133)	120π131π**132π**-134π135π137π	122π123σ128σ-134π135π143π

In the Pauling's or Allen's scales of electronegativity (EN) we have that EN(C) < EN(N) < EN(O). Therefore, it is expected that the net charge of atom 19 be positive. Table 17 shows three interesting facts. The first one is that $LUMO_{19}^{*}$ does coincide with the molecular LUMO and has a π nature in all molecules. The second fact is that $HOMO_{19}^{*}$ never coincides with the molecular HOMO. Also, in several cases it corresponds to occupied MOs with an energy located very far below from the HOMO energy. The last fact is that the nature of $HOMO_{19}^{*}$ can be π or σ. A high inhibitory activity is associated with low negative values of μ_{19}. Noting that this local reactivity index is the midpoint between the energies of $HOMO_{19}^{*}$ and $LUMO_{19}^{*}$, low negative values are obtained by shifting upwards the $HOMO_{19}^{*}$ energy, shifting upwards the $LUMO_{19}^{*}$ energy, or by a combination of both procedures. There is not a rigorous reason to select anyone of them. In the case when $HOMO_{19}^{*}$ is very close to the molecular HOMO, shifting upwards the $HOMO_{19}^{*}$'s energy will lead to a low negative value for μ_{19}. In this case this MO will become more reactive. Table 7 shows that all the $HOMO_{19}^{*}$ meeting this condition have all a σ nature, and could be involved in σ-σ or σ-π interactions. If we shift upwards the $LUMO_{19}^{*}$ energy, we are making this MO less prone to interact with an electron rich center. Now, if we consider that atom 19 has a positive net charge we expect that it interacts with an electron rich center or with a negatively charged moiety. For the moment, the method employed here does not allow us to carry out a deeper analysis. The situation is also complicated by the fact that this reactivity index has a very low *p*-value (Table 3). Atom 1 is a carbon in ring A (Fig. 2). The three highest occupied and the three lowest vacant local MOs are of π nature in all molecules (Table 11). If the numerical values of $S_1^N(LUMO+1)^*$ are positive, a high inhibitory activity is associated with high values of this index. Therefore we suggest that atom 1 is interacting with an electron rich center through the first two lowest vacant MOs. Despite the fact that this local reactivity index also has a low *p*-value (Table 3), and contrary to the case of μ_{19}, we are able to propose a definite atom-site interaction. All the suggestions are shown in the partial planar (2D) pharmacophore of Fig. 7.

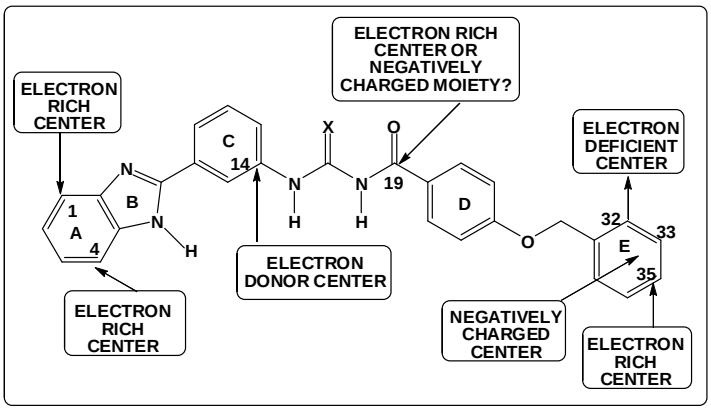

Figure 7. Partial 2D pharmacophore for the *in vitro* cell growth inhibition of the human HT29 cancer cell line

We can see in Fig. 7 that practically all the common skeleton is involved in the antiproliferative effect. The fact that in rings A and E several indices appear is a strong indirect evidence that these rings could be involved in ring-ring (π-π) interactions with the site. No direct evidence of hydrogen bond formation was found.

Discussion of MGC803 results

Beta values (Table 5) show that the importance of variables is S_{35}^{E}>> S_{32}^{E}> $S_{15}^{E}(HOMO-1)*$>> $S_{25}^{N}(LUMO+2)*$> $S_{18}^{N}(LUMO+1)*$> $S_{23}^{N}(LUMO+1)*$> $S_{24}^{E}(HOMO-1)*$. Eq. 2 shows that a high antiproliferative capacity is associated with high numerical values of $\left|S_{15}^{E}(HOMO-1)*\right|$ and $\left|S_{24}^{E}(HOMO-1)*\right|$, and with low numerical values of $\left|S_{35}^{E}\right|$ and $\left|S_{32}^{E}\right|$. The nature of the contribution of the nucleophilic superdelocalizabilities will be discussed case by case. Atom 35 is a carbon atom belonging to ring E. A low numerical value for $\left|S_{35}^{E}\right|$ suggests that this atom should behave as a bad electron donor. Therefore, we suggest that atom 35 is interacting with an electron rich center. Atom 32 is a carbon atom belonging to ring E. A low numerical value for $\left|S_{32}^{E}\right|$ suggests that this atom should behave as a bad electron donor. Therefore, we suggest that atom 32 is also interacting with an electron rich center. Atom 15 is a carbon atom belonging to ring C. High antiproliferative activity is associated with high negative values for $S_{15}^{E}(HOMO-1)*$. $(HOMO-1)_{15}^{*}$ and $HOMO-1_{15}^{*}$ have a π nature in all molecules (Table 12). We suggest then that atom 15 is interacting with an electron deficient center. Atom 25 is a carbon atom belonging to ring D. If the numerical values of $S_{25}^{N}(LUMO+2)*$ are positive, then low values for this reactivity index are associated with high antiproliferative activity. Table 14 shows that the three lowest vacant local MOs are of π nature. Low values for $S_{25}^{N}(LUMO+2)*$ are obtained by shifting upwards the $(LUMO+2)_{25}^{*}$ energy or by diminishing the value of the associated Fukui index (i.e., by minimizing the localization of $(LUMO+2)_{25}^{*}$ on this atom). We think that this requirement could be due to the repulsive interaction of this specific MO with empty MOs of the site. Therefore, we suggest that atom 25 is interacting with an electron rich center through its first two vacant MOs. This is indirectly supported by the fact that the local HOMO corresponds in all cases to an occupied MO located far from the molecule's HOMO. The analysis for the case of negative numerical values leads to an identical result. Atom 18 is the underlined nitrogen atom of the NC(X)NC(O) moiety linking rings C and D (Fig. 2). Table 13 shows that the first three lowest vacant MOs are of π nature. A high antiproliferative activity is associated with small values if $S_{18}^{N}(LUMO+1)*$ is positive and with high negative values if $S_{18}^{N}(LUMO+1)*$ is negative. In both cases this requirement is satisfied by shifting upwards the $(LUMO+1)_{18}^{*}$ energy and/or by diminishing the degree of localization of this MO on this atom. $HOMO_{18}^{*}$ can be of σ or π nature. Only with this available information we can suggest that atom 18 could be interacting with an electron rich center through its first vacant MO ($LUMO_{18}^{*}$). Note that we have included the local reactivity indices of H38 (bonded to N18, Fig. 2) to explore the possibility of formation of a hydrogen bond, but no statistically significant index appeared in Eq. 2. Atom 23 is a carbon atom belonging to ring D. If the value of $S_{23}^{N}(LUMO+1)*$ is positive, a high antiproliferative activity is associated with low values for this index. Table 14 shows that the local $HOMO^{*}$s do not coincide with the molecular HOMO in all the molecules. In the case of the local $LUMO^{*}$s, they

coincide with the molecular LUMO. The first three occupied and the first three vacant MOs have all a π nature (Table 14). As discussed above this suggests that atom 23 is interacting with an electron rich moiety through its first vacant local MO and that possibly the second vacant MO is engaged in a repulsive interaction with empty MOs of the partner. Atom 24 is a carbon atom belonging to ring D. A high antiproliferative activity is associated with high negative values for $S_{24}^{E}(HOMO-1)*$. Table 14 shows that the first three occupied and the first three vacant local MOs have all a π nature. Despite the fact that the local HOMO*s do not coincide with the molecular HOMO in all the cases analyzed here, we suggest that atom 24 is interacting with an electron deficient center through its first two highest occupied local MOs. All the suggestions are presented in the partial 2D pharmacophore of Fig. 8.

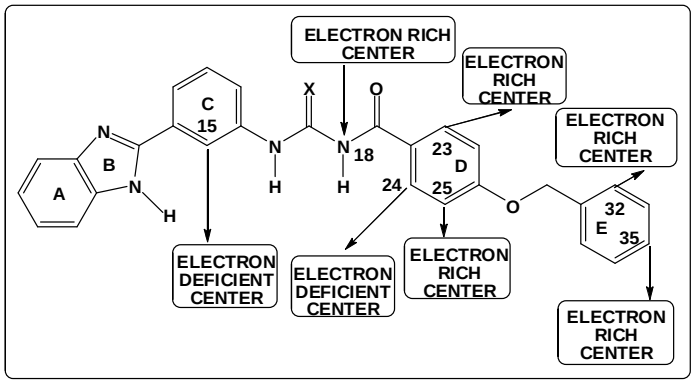

Figure 8. Partial 2D pharmacophore for the *in vitro* cell growth inhibition of the human MGC803 cancer cell line

We can see that LARIs belonging to rings A and B do not appear. This does not mean that there rings do not interact with the site. The presence of several LARISs of rings D and E is, as we said before, an indirect evidence that these rings could be involved in ring-ring (π-π) interactions with the site. No direct evidence of hydrogen bond formation was found.

Discussion of MKN45 results

Beta values (Table 7) show that the importance of variables is $S_{35}^{E} > S_{13}^{N}(LUMO+1)* > S_{27}^{N}(LUMO+2)* > S_{25}^{E}(HOMO-1)* > S_{24}^{E}(HOMO-1)* > S_{11}^{N}(LUMO+2)* > S_{31}^{N}(LUMO+1)* > S_{21}^{E}(HOMO-1)*$. Eq. 3 shows that a high antiproliferative capacity is associated with great negative values for $S_{25}^{E}(HOMO-1)*$, $S_{24}^{E}(HOMO-1)*$ and $S_{21}^{E}(HOMO-1)*$; and with small negative values for S_{35}^{E}. The nature of the contribution of the nucleophilic superdelocalizabilities will be discussed case by case. Atom 13 is a carbon atom belonging to ring C (Fig. 2). Table 12 shows that the three highest occupied and the three lowest vacant MOs have a π nature. If the values of $S_{13}^{N}(LUMO+1)*$ are positive, a high antiproliferative activity is associated with great numerical values for this index. High values are obtained by shifting downwards the $(LUMO+1)_{13}^{*}$ energy, making this MO more reactive. Therefore, we suggest that atom 13 is interacting with an electron rich center through its first two vacant MOs. For negative values of $S_{13}^{N}(LUMO+1)*$ the analysis leads to the same conclusion. Atom 35 is a carbon atom belonging to ring E (Fig. 2). A high antiproliferative activity is associated with low negative numerical values for this index (let us remember that the total atomic electrophilic superdelocalizability is always negative for closed shell, neutral molecules). Therefore, we suggest that atom 35 is interacting with an electron rich center. Atom 27 is a carbon atom belonging to ring D (Fig. 2). If the values of $S_{27}^{N}(LUMO+2)*$ are positive, a high antiproliferative activity is associated with low numerical values for this index. This means that $(LUMO+2)_{27}^{*}$ seems to be engaged in a repulsive interaction with vacant MOs of the partner. Table 15 shows that the three highest occupied and the three lowest vacant MOs have a π nature. We suggest that atom 27 is engaged in an interaction with an electron rich center through its first two lowest vacant MOs. This is indirectly supported by the fact that $(HOMO)_{27}^{*}$ does not coincide with the molecular HOMO, making it difficult that atom 27 acts as an electron donor. Atom 25 is a carbon atom belonging to ring D (Fig. 2). A high antiproliferative activity is associated with great negative values for $S_{25}^{E}(HOMO-1)*$. Table 14 shows that the three highest occupied and the three lowest vacant local MOs have a π nature. Therefore, it is suggested that atom 25 interacts with an electron deficient center through its first two highest occupied local MOs. Atom 24 is a carbon atom belonging to ring D (Fig. 2). A high antiproliferative activity is associated with great negative values for $S_{24}^{E}(HOMO-1)*$. Table 14 shows that the

three highest occupied and the three lowest vacant local MOs have a π nature. Therefore, we suggest that atom 24 interacts with an electron deficient center through its first two highest occupied local MOs. Atom 31 is a carbon atom belonging to ring E (Fig. 2). Table 16 shows that the three highest occupied and the three lowest vacant local MOs have a π nature. If the values of $S_{31}^{N}(LUMO+1)*$ are positive, a high antiproliferative activity is associated with high numerical values for this index. This, in turn, makes $(LUMO+1)_{31}{}^{*}$ more reactive. Then, atom 31 seems to interact with an electron rich center. Atom 11 is a carbon atom belonging to ring C (Fig. 2). If the values of $S_{11}^{N}(LUMO+2)*$ are positive, then a high antiproliferative activity is associated with small values for this index. This suggests that $(LUMO+2)_{11}{}^{*}$ is engaged in a repulsive interactions with vacant MOs of the partner. On the other hand, Table 11 shows that the three highest occupied and the three lowest vacant local MOs have a π nature and that the local frontier MOs coincide with the molecular ones. A preliminary suggestion is that atom 11 interacts with an electron rich site through its first two lowest vacant MOs. Atom 21 is the underlined oxygen atom of the NC(X)NC(O) moiety linking rings C and D (Fig. 2). Table 13 shows that the three highest occupied and the three lowest vacant local MOs have a π nature. A high antiproliferative activity is associated with great (negative) values of $S_{21}^{E}(HOMO-1)*$. This is a hint allowing us to suggest that atom 21 is interacting with an electron deficient center through its first two highest occupied local MOs. All the suggestions are presented in the partial 2D pharmacophore of Fig. 9.

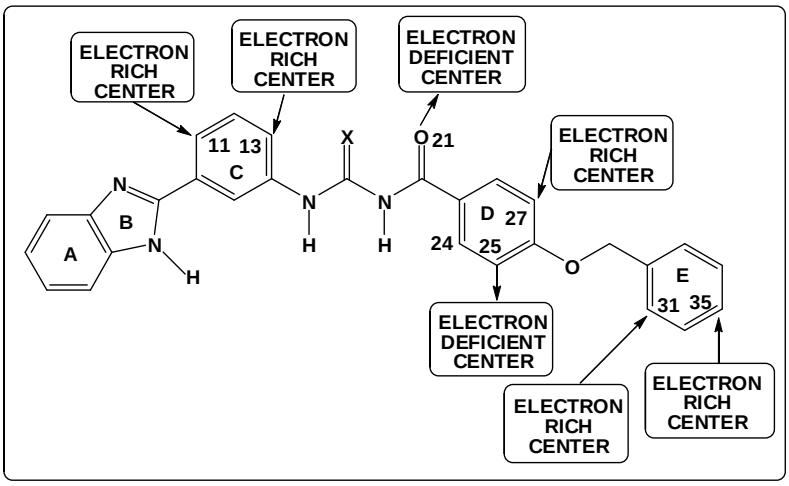

Figure 9. Partial 2D pharmacophore for the *in vitro* cell growth inhibition of the human MKN45 cancer cell line

We can see that LARIs belonging to rings A and B do not appear like in the MGC803 case. Here we also find indirect evidence of ring-ring (π-π) interactions in the case of rings C, D and E. No direct evidence of hydrogen bond formation was found.

Discussion of SW620 results

Beta values (Table 9) show that the importance of variables is $Q_{32} > S_{17}^{N}(LUMO)* > \mu_{34} > S_{12}^{E}(HOMO-2)* > F_{31}(LUMO)* > F_{32}(LUMO)*$. Eq. 4 shows that a high antiproliferative capacity is associated with a positive net charge on atom 32, great negative values for μ_{34} and $S_{12}^{E}(HOMO-2)*$, great positive values for $F_{31}(LUMO)*$ and small positive values for $F_{32}(LUMO)*$. Eq. 4 shows that a high antiproliferative activity is associated with a positive net charge on atom 32, suggesting that atom is engaged in an electrostatic interaction with a negatively charged site. Note that Table 15 shows that the local HOMO*s are far below the molecular HOMO. Atom 17 is the underlined carbon atom of the N<u>C</u>(X)NC(O) moiety linking rings C and D (Fig. 2). Table 13 shows that that the three highest occupied and the three lowest vacant local MOs have a π nature. If $S_{17}^{N}(LUMO)*$ is positive, then a high antiproliferative activity is associated with high values for this index. Therefore, we suggest that atom 17 is interacting with an electron rich center through its first lowest vacant local MO. Atom 34 is a carbon atom belonging to ring E (Fig. 2). Table 16 shows that the three highest occupied and the three lowest vacant local MOs have a π nature. A high antiproliferative activity is associated with great negative values for μ_{34}. For this reason it is suggested that atom 34 is interacting with an electron rich center with at least its lowest vacant local MO. Atom 12 is a carbon atom belonging to ring C (Fig. 2). Table 12 shows that the

three highest occupied and the three lowest vacant local MOs have a π nature. A high antiproliferative activity is associated with higher (negative) values of $S_{12}^{E}(HOMO-2)^{*}$. We suggest then that atom 12 is interacting with an electron deficient center with, at least, its three highest occupied local MOs. Atom 31 is a carbon atom belonging to ring E (Fig. 2). Table 15 shows that the three highest occupied and the three lowest vacant local MOs have a π nature. A high antiproliferative activity is associated with high values of $F_{31}(LUMO)^{*}$ (the Fukui index is always greater than zero [75]). This allow us to suggest that atom 31 is interacting with an electron rich center through its first lowest vacant local MO. Atom 32 is a carbon atom belonging to ring E (Fig. 2). Table 15 shows that the three highest occupied and the three lowest vacant local MOs have a π nature. A high antiproliferative activity is associated with low values of $F_{32}(LUMO)^{*}$. This suggests that $LUMO_{32}^{*}$ is engaged in a repulsive interaction with a vacant MO of the site. Our preliminary suggestion is that atom 32 is interacting with an electron deficient center. This is contradictory with the requirement for Q_{32}. Considering the low p-value associated to $F_{32}(LUMO)^{*}$ we shall not consider this possibility. All the suggestions are displayed in the partial 2D pharmacophore of Fig. 10.

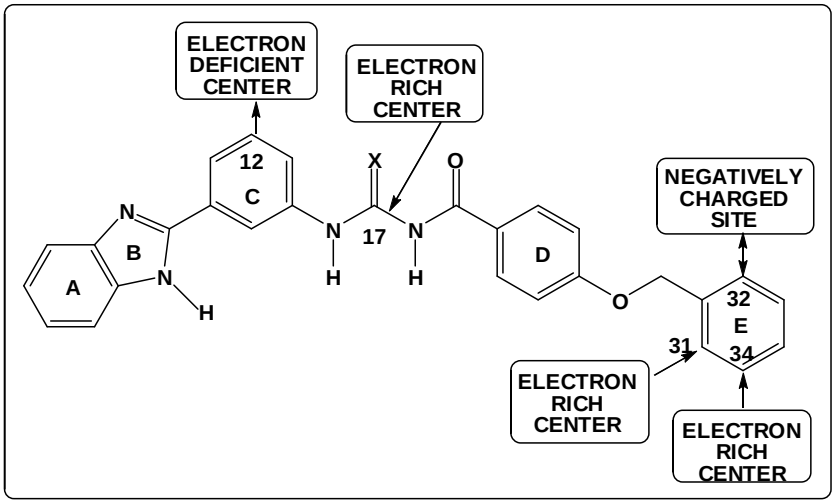

Figure 10. Partial 2D pharmacophore for the *in vitro* cell growth inhibition of the human SW620 cancer cell line

Again, LARIs belonging to rings A and B do not appear. In this case there is indirect evidence of a ring-ring (π-π) interaction is found for ring E. No direct evidence of hydrogen bond formation was found.

The substituent effects are of three kinds. The first one is the so-called orientational effect of the substituent, having not electronic components, and developed directly from the molecular rotational partition function [39]. This orientational effect influences the distribution of the molecule's rotation velocity (in a classical temperature-dependent distribution scheme) and how the molecule rotates about its three principal axis of rotation. The second kind corresponds to concepts such as resonance and inductive effects, developed by XX century organic chemistry. The third one is more subtle and is related to the form of the solutions of the Hartree-Fock and Kohn-Sham equations. These equations provide molecular orbital structures in terms of a linear combination of atomic orbitals (AO). The set of AOs employed (i.e., the basis set) may vary considerably. For example, if we change a methyl by an ethyl substituent we shall introduce more atomic orbitals and more molecular orbitals will appear in the final results. The question is that in the case of big molecules (such as the ones analyzed in this paper) changing a given substituent by another similar may change, not only the nature of the molecular orbitals close to the frontier ones (HOMO and LUMO), but the localization of some of them. This is the reason why we include in the LMRA at least the three highest occupied and the three lowest vacant local MOs [37, 38]. Regarding the second kind of substituent effects, we are sure that they can be explained through quantum chemistry studies with local atomic reactivity indices and that one day their unique use will be only for teaching. The paper reporting the measured antiproliferative activities could be taken as an example containing quite primitive statements to design molecules. "*To further improve the activity by altering the distribution of electrons in ring B, we incorporated the methyl group but this attempt was a failure*" and "*however, the trend was not sustained, as other disubstituted analogues were either less potent or inactive*" are good examples. We think that if after measuring the activities, a full quantum-chemical analysis were performed, probably new similar compounds with improved activity will see the light of day. On the other hand, the question of obtaining the LARIs deserves some words. We normally use Mulliken's

population analysis results after correcting them to eliminate negative electron populations or MO populations greater than 2 [71]. Any other population analysis scheme can be used. Finally, the question of knowing if the role of the C-E rings connector is the same for all the cases analyzed here cannot be fully answered.

In summary, we have found statistically significant equations relating electronic structure with antiproliferative activity in four cancer cell lines. The corresponding 2D pharmacophores are built and some ring-ring interactions are suggested. The analysis of the equations and the pharmacophores should provide information about new possible substitution sites.

REFERENCES

[1] L Zhao, J-J Zhou, X-Y Huang, L-P Cheng, W Pang, et al., *Chin. Chem. Lett.*, **2015**, 26, 993-999.
[2] Y-F Win, C-S Choong, J-C Dang, MA Iqbal, CK Quah, et al., *Comp. Rend. Chim.*, **2015**, 18, 137-148.
[3] M Vergara, A Olivares, C Altamirano, *Electr. J. Biotech.*, **2015**, 18, 291-294.
[4] LF Toneto Novaes, C Martins Avila, KJ Pelizzaro-Rocha, DB Vendramini-Costa, M Pereira Dias, et al., *ChemMedChem*, **2015**, 10, 1687-1699.
[5] C Sun, Y Li, A Shi, J Zhang, Y Li, et al., *MedChemComm*, **2015**, 6, 1137-1142.
[6] K Pant, A Gupta, P Gupta, A Ashraf, A Yadav, et al., *J. Clin. Exp. Hepatol.*, **2015**, 5, Supplement 2, S2.
[7] A Manosroi, H Akazawa, T Akihisa, P Jantrawut, W Kitdamrongtham, et al., *J. Ethnopharm.*, **2015**, 161, 11-17.
[8] JA Lawrence, MK Huelsmeyer, DH Thamm, DB Tumas, G Birkus, et al., *Vet. Comp. Oncol.*, **2015**, 13, 246-254.
[9] I Karpavičienė, G Valiulienė, V Raškevičius, I Lebedytė, A Brukštus, et al., *Eur. J. Med. Chem.*, **2015**, 98, 30-48.
[10] TK-D Hoang, TK-C Huynh, T-D Nguyen, *Bioorg. Chem.*, **2015**, 63, 45-52.
[11] N Hatae, E Fujita, S Shigenobu, S Shimoyama, Y Ishihara, et al., *Bioorg. Med. Chem. Lett.*, **2015**, 25, 2749-2752.
[12] MJ Ferronato, DG Salomón, ME Fermento, NA Gandini, A López Romero, et al., *Arch. Pharmaz.*, **2015**, 348, 315-329.
[13] N Ferri, G Facchetti, S Pellegrino, C Ricci, G Curigliano, et al., *Bioorg. Med. Chem.*, **2015**, 23, 2538-2547.
[14] O Catchpole, K Mitchell, S Bloor, P Davis, A Suddes, *Fitoter.*, **2015**, 106, 167-174.
[15] M Carraz, C Lavergne, V Jullian, M Wright, JE Gairin, et al., *J. Ethnopharm.*, **2015**, 166, 185-199.
[16] BCB Boaventura, RDdMC Amboni, EL da Silva, ES Prudencio, PF Di Pietro, et al., *Food Res. Int.*, **2015**, 77, Part 2, 257-263.
[17] E Venkateswararao, VK Sharma, M Manickam, J Yun, S-H Jung, *Bioorg. Med. Chem. Lett.*, **2014**, 24, 5256-5259.
[18] KS Sharath Kumar, A Hanumappa, M Hegde, KH Narasimhamurthy, SC Raghavan, et al., *Eur. J. Med. Chem.*, **2014**, 81, 341-349.
[19] P Sarkar, S Maiti, K Ghosh, S Sengupta, RJ Butcher, et al., *Tet. Lett.*, **2014**, 55, 996-1001.
[20] U Reddy Chamakura, E Sailaja, B Dulla, AM Kalle, S Bhavani, et al., *Bioorg. Med. Chem. Lett.*, **2014**, 24, 1366-1372.
[21] NR Madadi, NR Penthala, V Janganati, PA Crooks, *Bioorg. Med. Chem. Lett.*, **2014**, 24, 601-603.
[22] A Leoni, A Locatelli, R Morigi, M Rambaldi, C Cappadone, et al., *Eur. J. Med. Chem.*, **2014**, 79, 382-390.
[23] M Hedidi, G Bentabed-Ababsa, A Derdour, T Roisnel, V Dorcet, et al., *Bioorg. Med. Chem.*, **2014**, 22, 3498-3507.
[24] B Dulla, E Sailaja, U Reddy Ch, M Aeluri, AM Kalle, et al., *Tet. Lett.*, **2014**, 55, 921-926.
[25] DV Demchuk, AV Samet, NB Chernysheva, VI Ushkarov, GA Stashina, et al., *Bioorg. Med. Chem.*, **2014**, 22, 738-755.
[26] J Defaux, M Antoine, C Logé, M Le Borgne, T Schuster, et al., *Bioorg. Med. Chem. Lett.*, **2014**, 24, 3748-3752.
[27] Ş Cankara Pirol, B Çalışkan, İ Durmaz, R Atalay, E Banoglu, *Eur. J. Med. Chem.*, **2014**, 87, 140-149.
[28] AH Banday, AK Giri, R Parveen, N Bashir, *Steroids*, **2014**, 87, 93-98.
[29] N Ahmed, NK Konduru, S Ahmad, M Owais, *Eur. J. Med. Chem.*, **2014**, 75, 233-246.
[30] N Ahmed, NK Konduru, S Ahmad, M Owais, *Eur. J. Med. Chem.*, **2014**, 82, 552-564.
[31] G Cebrián-Torrejón, A Doménech-Carbó, MT Scotti, A Fournet, B Figadère, et al., *J. Mol. Struct*,, **2015**, 1102, 242-246.
[32] JS Gómez-Jeria, A Robles-Navarro, *Res. J. Pharmac. Biol. Chem. Sci.*, **2015**, 6, 755-783.
[33] DI Pino-Ramírez, JS Gómez-Jeria, *Amer. Chem. Sci. J.*, **2014**, 4, 554-575.
[34] JS Gómez-Jeria, *Der Pharma Chem.*, **2014**, 6, 64-77.
[35] F Gatica-Díaz, JS Gómez-Jeria, *J. Comput. Methods Drug Des.*, **2014**, 4, 79-120.
[36] JS Gómez-Jeria, M Flores-Catalán, *Canad. Chem. Trans.*, **2013**, 1, 215-237.

[37] JS Gómez-Jeria, *Canad. Chem. Trans.*, **2013**, 1, 25-55.
[38] JS Gómez-Jeria, *Elements of Molecular Electronic Pharmacology (in Spanish)*, Ediciones Sokar, Santiago de Chile, 2013.
[39] JS Gómez-Jeria, M Ojeda-Vergara, *J. Chil. Chem. Soc.*, **2003**, 48, 119-124.
[40] JS Gómez-Jeria, M Ojeda-Vergara, C Donoso-Espinoza, *Mol. Engn.*, **1995**, 5, 391-401.
[41] JS Gómez-Jeria, "Modeling the Drug-Receptor Interaction in Quantum Pharmacology," in *Molecules in Physics, Chemistry, and Biology*, J. Maruani Ed., vol. 4, pp. 215-231, Springer Netherlands, 1989.
[42] JS Gómez-Jeria, *Int. J. Quant. Chem.*, **1983**, 23, 1969-1972.
[43] JS Gómez Jeria, *Boll. Chim. Farmac.*, **1982**, 121, 619-625.
[44] F Salgado-Valdés, JS Gómez-Jeria, *J. Quant. Chem.*, **2014**, 2014 Article ID 431432, 1-15.
[45] YC Martin, *Quantitative drug design: a critical introduction*, M. Dekker, New York, 1978.
[46] J Valdebenito-Gamboa, JS Gómez-Jeria, *Der Pharma Chem.*, **2015**, 7, 543-555.
[47] MS Leal, A Robles-Navarro, JS Gómez-Jeria, *Der Pharm. Lett.*, **2015**, 7, 54-66.
[48] JS Gómez-Jeria, J Valdebenito-Gamboa, *Der Pharma Chem.*, **2015**, 7, 323-347.
[49] JS Gómez-Jeria, J Valdebenito-Gamboa, *Der Pharm. Lett.*, **2015**, 7, 211-219.
[50] JS Gómez-Jeria, A Robles-Navarro, *Res. J. Pharmac. Biol. Chem. Sci.*, **2015**, 6, 1358-1373.
[51] JS Gómez-Jeria, A Robles-Navarro, *Res. J. Pharmac. Biol. Chem. Sci.*, **2015**, 6, 1811-1841.
[52] JS Gómez-Jeria, A Robles-Navarro, *J. Comput. Methods Drug Des.*, **2015**, 5, 15-26.
[53] JS Gómez-Jeria, A Robles-Navarro, *Der Pharma Chem.*, **2015**, 7, 243-269.
[54] JS Gómez-Jeria, A Robles-Navarro, *Res. J. Pharmac. Biol. Chem. Sci.*, **2015**, 6, 1337-1351.
[55] JS Gómez-Jeria, *Res. J. Pharmac. Biol. Chem. Sci.*, **2015**, 6, 688-697.
[56] R Solís-Gutiérrez, JS Gómez-Jeria, *Res. J. Pharmac. Biol. Chem. Sci.*, **2014**, 5, 1401-1416.
[57] D Muñoz-Gacitúa, JS Gómez-Jeria, *J. Comput. Methods Drug Des.*, **2014**, 4, 48-63.
[58] D Muñoz-Gacitúa, JS Gómez-Jeria, *J. Comput. Methods Drug Des.*, **2014**, 4, 33-47.
[59] JS Gómez-Jeria, J Valdebenito-Gamboa, *Der Pharma Chem.*, **2014**, 6, 383-406.
[60] JS Gómez-Jeria, J Molina-Hidalgo, *J. Comput. Methods Drug Des.*, **2014**, 4, 1-9.
[61] JS Gómez-Jeria, *Res. J. Pharmac. Biol. Chem. Sci.*, **2014**, 5, 780-792.
[62] JS Gómez-Jeria, *J. Comput. Methods Drug Des.*, **2014**, 4, 38-47.
[63] JS Gómez-Jeria, *Res. J. Pharmac. Biol. Chem. Sci.*, **2014**, 5, 424-436.
[64] JS Gómez-Jeria, *J. Comput. Methods Drug Des.*, **2014**, 4, 32-44.
[65] JS Gómez-Jeria, *Res. J. Pharmac. Biol. Chem. Sci.*, **2014**, 5, 2124-2142.
[66] JS Gómez-Jeria, *SOP Trans. Phys. Chem.*, **2014**, 1, 10-28.
[67] JS Gómez-Jeria, *Brit. Microbiol. Res. J.*, **2014**, 4, 968-987.
[68] JS Gómez-Jeria, *Der Pharm. Lett.*, **2014**, 6., 95-104.
[69] JS Gómez-Jeria, *Int. Res. J. Pure App. Chem.*, **2014**, 4, 270-291.
[70] MJ Frisch, GW Trucks, HB Schlegel, GE Scuseria, MA Robb, et al., "G03 Rev. E.01," Gaussian, Pittsburgh, PA, USA, **2007**.
[71] JS Gómez-Jeria, *J. Chil. Chem. Soc.*, **2009**, 54, 482-485.
[72] RS Mulliken, *J. Chem. Phys.*, **1955**, 23, 1833-1840.
[73] JS Gómez-Jeria, "D-Cent-QSAR: A program to generate Local Atomic Reactivity Indices from Gaussian 03 log files. 1.0," Santiago, Chile, **2014**.
[74] Statsoft, "Statistica 8.0," 2300 East 14 th St. Tulsa, OK 74104, USA, **1984**-2007.
[75] K Fukui, H Fujimoto, *Frontier orbitals and reaction paths: selected papers of Kenichi Fukui*, World Scientific, Singapore; River Edge, N.J., **1997**.